Electron and Ion Dynamics of the Solar Wind Interaction with a Weakly Outgassing Comet

Jan Deca,[1,2,*] Andrey Divin,[3,4] Pierre Henri,[5] Anders Eriksson,[4] Stefano Markidis,[6] Vyacheslav Olshevsky,[7] and Mihály Horányi[1,2]

[1]*Laboratory for Atmospheric and Space Physics (LASP), University of Colorado Boulder, Boulder, Colorado 80303, USA*
[2]*Institute for Modeling Plasma, Atmospheres and Cosmic Dust, NASA/SSERVI, Moffett Field, California 94035, USA*
[3]*Physics Department, St. Petersburg State University, St. Petersburg 198504, Russia*
[4]*Swedish Institute of Space Physics (IRF), Uppsala 751 21, Sweden*
[5]*LPC2E, CNRS, Orléans 45071, France*
[6]*KTH Royal Institute of Technology, Stockholm 100 44, Sweden*
[7]*Centre for mathematical Plasma Astrophysics (CmPA), KU Leuven, Leuven 3001, Belgium*

(Received 8 February 2017; published 15 May 2017; publisher error corrected 5 June 2017)

Using a 3D fully kinetic approach, we disentangle and explain the ion and electron dynamics of the solar wind interaction with a weakly outgassing comet. We show that, to first order, the dynamical interaction is representative of a four-fluid coupled system. We self-consistently simulate and identify the origin of the warm and suprathermal electron distributions observed by ESA's Rosetta mission to comet 67P/Churyumov-Gerasimenko and conclude that a detailed kinetic treatment of the electron dynamics is critical to fully capture the complex physics of mass-loading plasmas.

DOI: 10.1103/PhysRevLett.118.205101

Cometary nuclei are small, irregularly shaped "icy dirt balls" left over from the dawn of our Solar System 4.6 billion years ago and are composed of a mixture of ices, refractory materials, and large organic molecules [1–4]. When a comet is sufficiently close to the Sun, the sublimation of ice leads to an outgassing atmosphere and the formation of a coma, and a dust and plasma tail. Historically, this process revealed the existence of the solar wind and the interplanetary magnetic field [5–8]. Comets are critical to decipher the physics of gas release processes in space. The latter result in mass-loaded plasmas [9,10], which more than three decades after the Active Magnetospheric Particle Tracer Explorers (AMPTE) space release experiments [11] are still not fully understood.

First observed in 1969, comet 67P/Churyumov-Gerasimenko was escorted for almost two years along its 6.45-yr elliptical orbit by ESA's Rosetta orbiter spacecraft. During the mission, the comet transitioned from its weakly outgassing phase into a more active object as it approached the Sun, and back again to quieter phases when traveling outward in the Solar System. This first ever mission to do more than a simple cometary fly-by revealed in unprecedented detail the fascinating evolution of a comet [12] and the building up of its induced magnetosphere [13].

To date, the focus of modeling studies to predict and explain the complex cometary plasma observations has been on magnetohydrodynamic (MHD) or multifluid [14–19] and hybrid (using a kinetic description for the ions but describing the electrons as a massless fluid) [20–26] simulations, leading to comprehensive models for the ion dynamics. A satisfactory explanation for the observed electron dynamics, however, is not yet available. For instance, the Ion and Electron Sensor (IES) instrument onboard the Rosetta orbiter shows the presence of nonthermal electron distributions inside the inhomogeneous expanding cometary ionosphere, including both a warm (∼5 eV) and suprathermal (10–20 eV) component [27–29]. The origin and physical mechanism behind the various components of the observed electron distributions is unclear, but must be understood to disentangle the cometary plasma dynamics.

We develop and analyze a detailed model of the cometary plasma dynamics, including fine-scale electron kinetic physics, and discuss the relative acceleration mechanisms decoupling the plasma populations. Using the collisionless semi-implicit, fully kinetic, electromagnetic particle-in-cell code iPIC3D [30], which solves the Vlasov-Maxwell system of equations for both ions and electrons using the implicit moment method [31–33], we focus on the interaction between the solar wind and a weakly outgassing comet such as encountered by Rosetta at approximately 3 astronomical units (A.U.). from the Sun. At such large distances from the Sun, the collisionless approximation is valid everywhere except in the innermost coma [34,35]. We model self-consistently the kinetic dynamics of both cometary water ions and electrons, produced by the ionization of the radially expanding and outgassing cometary atmosphere, together with the incoming solar wind proton and electron plasma flow. To accommodate a flowing plasma in the computational domain, we use open boundary conditions as implemented by Deca *et al.* [36].

Maxwellian distributions of solar wind protons and electrons are injected at the inflow boundary of the

computational domain (at $x = -1540$ km) with densities $n_{p,sw} = n_{e,sw} = 1$ cm^{-3} and temperatures $T_{p,sw} = 7$ eV, $T_{e,sw} = 10$ eV, respectively, approximating the free-streaming solar wind plasma distributions [29,37]. The solar wind flows along X at $\mathbf{v}_{sw} = (400, 0, 0)$ km s^{-1}. We use a reduced mass ratio $m_{p,sw}/m_{e,sw} = 100$ to meet our numerical restrictions, a common practice in fully kinetic simulations that ensures scale separation between electron and ion dynamics [38]. The interplanetary magnetic field is directed along Y at $\boldsymbol{B}_{\mathrm{IMF}} = (0, 6, 0)$ nT, resulting in a solar wind proton and electron Larmor radius of $r_{p,sw} = 142$ km and $r_{e,sw} = 12$ km, respectively. The nucleus of the comet is represented by an absorbing sphere placed 110 km upstream of the center of the computational domain (at $(x, y, z) = (-110, 0, 0)$ km). The computational domain measures $3300 \times 2200 \times 2200$ km^3 with a resolution of 10 km in all three Cartesian directions. The simulation time step is $\Delta t = 4.5 \times 10^{-5}$ s, which is well below the electron gyroperiod (5.95 ms for 6 nT) and, hence, resolves the electron gyromotion.

The solar wind is mass loaded by cold cometary ions as a consequence of the outgassing cometary neutral atmosphere that is ionized as it expands [39]. In order to inject cometary ion-electron pairs, we do not implement the neutral gas distribution. Instead, we use an analytical profile for the plasma production rate that results from the ionization of an expanding neutral gas with a $1/r^2$ radial density profile. We assume a gas production rate of $Q = 10^{26}$ s^{-1} [40]. The resulting cometary density profile then mimics the $1/r$ plasma density profile observed close to the cometary nucleus [41]. We radially inject Maxwell-distributed cometary electrons ($T_{e,c} = 10$ eV) and cold cometary water group ions ($m_{i,c}/m_{p,sw} = 20$) accordingly. The thermal velocity of the implanted water ions is set 2 orders of magnitude smaller than the solar wind protons, which translates to a cometary ion temperature of $T_{i,c} = 0.5$ eV. Although $T_{i,c}$ is somewhat higher than observed by Rosetta (see, e.g., Nilsson *et al.* [13]), cometary ions are born in the simulation with energies 2000 times less than the solar wind energy, ensuring sufficient separation of scales.

Figure 1 shows the density profiles in the XY (terminator) and XZ (cross magnetic field) planes for the solar wind [Figs. 1(a)–1(d)] and cometary [Figs. 1(e)–1(h)] ion and electron species. The simulated global structure of the solar wind-weak comet interaction confirms the results reported by hybrid simulations on the induced cometary magnetosphere [23–25]. In particular, we observe a magnetic pileup (a direct consequence of the ionization of outflowing gas from the nucleus) up to more than 3 times the interplanetary magnetic field magnitude [42], together with a compression of the incoming, mass-loaded, solar wind [Fig. 1(a)]. The magnetic field lines drape around the nucleus. No bow shock develops, as expected for a weakly outgassing comet [22]. The heavy cometary ions are accelerated by the convective electric field, to be eventually picked up far downstream, whereas solar wind protons deflect in the opposite direction in accordance with momentum conservation. Downstream of the nucleus, Figs. 1(d) and 1(g) show a fanlike structure [15] and density fluctuations or filamentation [43] that can be associated with the so-called "singing comet" waves [25].

Focusing on the electron dynamics next [Figs. 1(b), 1(d), 1(f), and 1(h)], we find that, to first order, the electrons behave as two separate fluids: a solar wind and a cometary electron fluid. We observe a spatial separation of the cometary electrons with respect to the cometary ions, and of the solar wind electrons with respect to the solar wind protons. Cometary electrons eventually end up neutralizing the solar wind protons, and solar wind electrons eventually neutralize the cometary ions.

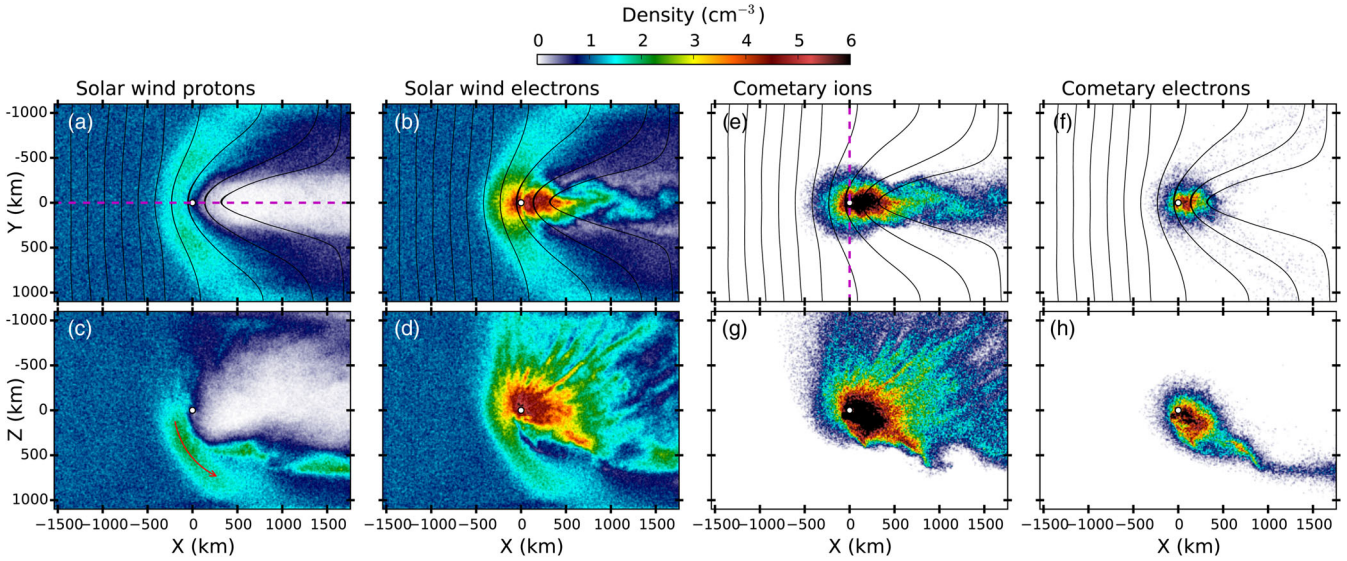

FIG. 1. Density profiles in the XY/XZ planes for the solar wind (left-hand panels) and cometary (right-hand panels) ions and electrons. The Y axis is directed along the solar wind magnetic field. Field lines are plotted in black. The red arrow in (c) indicates the deflected solar wind proton flow in the XZ plane.

The four species interact as follows. First, as cometary ions accelerate along the convective electric field in the cross magnetic field direction, cometary electrons are initially accelerated in the opposite direction. They are picked up into the solar wind flow much faster than the cometary ions, at scales larger than the electron gyroradius (~10 km). In other words, cometary electrons reach the solar wind flow velocity very locally (quickly) as compared to the cometary ions. This process spatially separates the cometary ion and electron dynamics. Second, this separation of the ion and electron motion results in a net current that is associated to a Hall electric field. Coupled to the need for quasineutrality at those scales, the solar wind electrons become decoupled from the solar wind protons upstream of the comet. At the same time, the convective electric field has an opposite sign in the solar wind and cometary ion reference frame and transfers momentum between the two species. While the solar wind protons are deflected, the interplanetary magnetic field continues to be carried close to the comet through the solar wind (and cometary) electrons as they are still frozen-in into the magnetic field. This behavior is quite similar to the ion diffusion region in magnetic reconnection [44].

From a kinetic point of view, the simulated four-fluid interaction, in particular, the separation of the solar wind and cometary electron dynamics, is coherent. Solar wind and cometary electrons populate different regions in phase space when close to the comet. They can therefore follow different phase-space trajectories. The velocity streamlines shown in Fig. 2 illustrate the four-fluid behavior.

The ability of our model to self-consistently describe the electron-kinetic dynamics of the solar wind-comet interaction shines new light on the (observed) particle energy distributions [29,45]. Figure 3 shows the solar wind, cometary, and total ion energy distributions along the Sun-comet direction (through the center of the computational domain; the cut is indicated in Fig. 1(a). The distributions are constructed by grouping the particle energies in uniform bins, collecting all particles per species available in $30 \times 30 \times 30$ km^3 cubic domains along the X direction. Figure 4 is constructed similarly, but along the Y axis of the domain.

Close to the cometary nucleus, no stagnation point is observed. Instead, the solar wind proton distribution loses part of its energy [Fig. 3(a)] as the incoming plasma is deflected when interacting with the cometary coma. The lost energy is transferred to the cometary ions that are picked up by the local convective electric field and accelerated tail ward [Fig. 3(b)]. This is qualitatively consistent with the observed energy behavior of the solar wind ions [46].

The cometary ion energy rises to 1000 eV in the solar wind proton wake behind the comet, a number comparable to the upstream solar wind proton energy [Fig. 3(c)]. Moving downstream and along the positive Z axis (not shown), however, we gradually encounter more energetic cometary ions as they are being picked up. At the edge of our computational domain the cometary ion population has already reached energies of 1750 eV. Eventually, far beyond our computational domain [15], the velocity of the cometary ion population will equal the solar wind flow

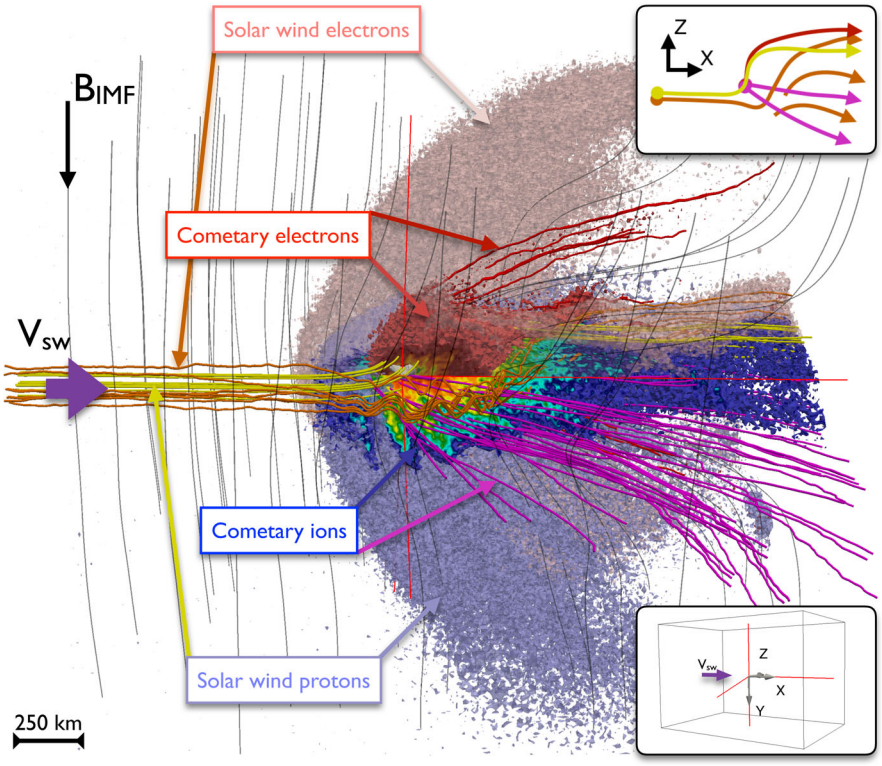

FIG. 2. 3D overview of the four-fluid behavior of the solar wind interaction with a weakly outgassing comet. Included in the illustration are the structure of the interplanetary magnetic field, density thresholds, and velocity streamlines for the four simulated species. The shape model of 67P/Churyumov-Gerasimenko is enlarged 5 times to increase visibility. The lower right-hand inset indicates how the density thresholds are cut. The upper right-hand inset illustrates the decoupling of the four species in the XZ plane, perpendicular to the interplanetary magnetic field.

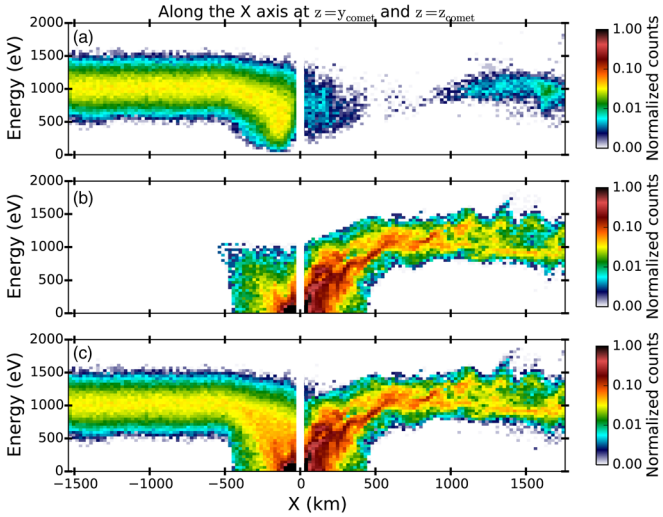

FIG. 3. Solar wind, cometary, and total (solar wind+ cometary) ion energy distributions along the Sun-comet direction [(a)–(c), respectively]. The cut is indicated in Fig. 1(a). The white band represents the comet location.

velocity ($T_{i,c} \rightarrow 20000$ eV, given our cometary ion mass ratio $m_{i,c}/m_{p,sw} = 20$).

We measure deflection angles in excess of 45° for both the solar wind protons and cometary ions. In addition, at a fixed location in space with respect to the comet, the pick-up angle is larger for cometary ions with greater energies [47]. Both observations are in agreement with recent plasma measurements by the Rosetta spacecraft [48,49].

Figure 4 shows the solar wind, cometary, and total electron energy distributions along a cut in the terminator plane [where Rosetta has resided most of the time; the cut is indicated in Fig. 1(e)]. Solar wind electrons accelerate

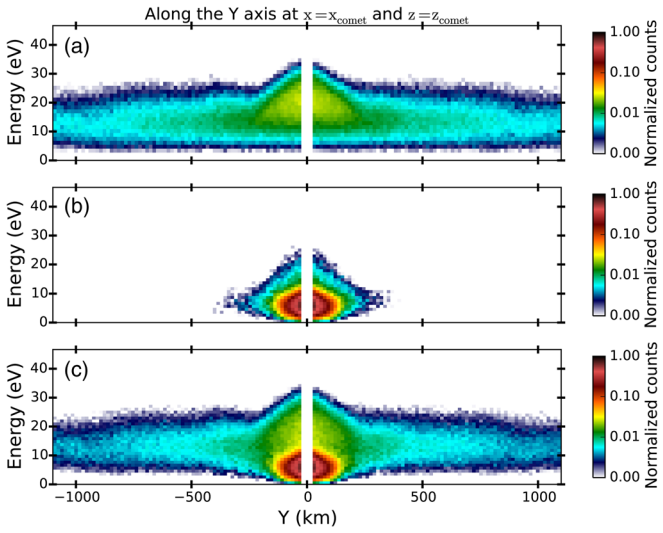

FIG. 4. Solar wind, cometary, and total (solar wind+ cometary) electron energy distributions along a cut in the terminator plane [(a)–(c), respectively]. The cut is indicated in Fig. 1(e). The white band represents the comet location.

towards the comet [Fig. 4(a)] under the influence of an ambipolar electric field that is generated by the large electron pressure gradient in the inhomogeneous cometary plasma [50], which further enhances the separation of the solar wind electron and ion flows. The total electron energy distribution [Fig. 4(c)] is once again the sum of Figs. 4(a) and 4(b). Close to the comet we observe a warm ~5-eV component of cometary origin and a 10–20-eV suprathermal component of solar wind origin. Our simulation self-consistently generates both components and reveals the origin of the two collisionless electron distributions observed by Rosetta in the cometary environment [27–29,45]. Note that a third, cold electron population has also been observed much closer to the Sun, when the electron-neutral collision rate, still negligible at 3 A.U., becomes high enough to cool down the warm cometary electrons [51].

Identifying the origin of the suprathermal electron population delivers clues to the physical mechanism behind their acceleration or heating in the collisionless coma. Two mechanisms have been discussed in literature thus far: (i) heating of electrons through wave particle interactions, such as the singing comet waves (understood as an ion Weibel instability [43,52]) or lower hybrid waves [45], and (ii) the acceleration of electrons along the ambipolar electric field [29]. In the second scenario, solar wind electrons traveling toward the comet fall into the potential well that is generated by the gradient in electron number density [53,54]. Electrons born inside, i.e., the cometary electrons, are trapped unless they carry enough energy to escape. The potential scales as the electron thermal energy [29]; hence, only suprathermal electrons will be able to escape the near-comet environment. Note that this interpretation is valid on subion time scales only, as quasineutrality will act such that electrons must eventually leave the potential well. Without ruling out the influence of wave particle interactions, our simulation favors the ambipolar electric field model, though this may not be the case at other activity phases of the comet.

We have focused here on a weakly outgassing cometary nucleus, where the plasma can be safely approximated as collisionless. We use the collisionopause or exobase distance, defined as the distance to the nucleus where the cometocentric distance equals the mean free path for collisions with neutrals, to characterize the validity of this assumption. For $Q = 10^{26}$ s^{-1}, we find the ion exobase at 3 km above the surface of the nucleus [35,51]. The electrons are collisionless down to the nucleus. Note that the ion value is computed here for very low energy ions, relevant for newborn ions inheriting the ~200 K temperature of the neutral gas. As the ion-neutral cross section rapidly decreases with energy, even a weak electric field combined with a high gas production rate may significantly decrease the ion collisionality [55]. Hence, while there may be some collisionality also in our case, we expect this to be the case only within the first few kilometers above the nucleus (not resolved in our simulation).

As the cometary outgassing activity increases, plasma-neutral collisions will play an increasingly significant role in shaping the ionized cometary environment. Collisions account for two significant processes in the context of mass-loaded plasmas: ion-neutral friction and electron cooling. When the gas production rate is high enough, plasma-neutral collisions eventually carve out a nonmagnetized region near the cometary nucleus [56]. This region is shaped by electron-neutral collisions [57]. Taking into account collisions will be necessary to extend this study for more active comets.

To conclude, we have produced the first 3D fully kinetic and electromagnetic simulations of the solar wind interaction with a weakly outgassing comet, for which the collisional interaction between the neutral gas and (mass-loading) plasma can be ignored, as is representative of comet 67P/Churyumov-Gerasimenko at 3 A.U. We have disentangled the collisionless electron- and ion-kinetic activity of the interaction and found that the electron dynamics, to first order, is that of two independent electron fluids. This allows us to interpret the main features and origin of the warm (cometary) and suprathermal (solar wind) electron distributions observed by the Rosetta mission. Although globally the dynamics of the solar wind-weak comet system is that of a four-fluid coupled system, we conclude that a multispecies electron-kinetic description is a must to fully capture the complex global solar wind-comet interaction process.

This work was supported in part by NASA's Solar System Exploration Research Virtual Institute (SSERVI): Institute for Modeling Plasmas, Atmosphere, and Cosmic Dust (IMPACT), and the NASA High-End Computing (HEC) Program through the NASA Advanced Supercomputing (NAS) Division at Ames Research Center. Part of this work was inspired by discussions within International Team 336: "Plasma Surface Interactions with Airless Bodies in Space and the Laboratory" at the International Space Science Institute, Bern, Switzerland. Work at LPC2E/CNRS was supported by CNES and by ANR under the financial agreement ANR-15-CE31-0009-01. Partial support is also acknowledged by Contract No. JPL-1502225 at the University of Colorado from Rosetta, which is an European Space Agency (ESA) mission with contributions from its member states and NASA.

*jandeca@gmail.com

[1] F. L. Whipple, Astrophys. J. **111**, 375 (1950).
[2] H. U. Keller, in *Physics and Mechanics of Cometary Materials*, ESA Special Publication Vol. 302, edited by J. J. Hunt and T. D. Guyenne (Westfälische Wilhems-Universität, Münster, 1989).
[3] W. M. Irvine, F. P. Schloerb, J. Crovisier, B. Fegley, Jr., and M. J. Mumma, *Protostars Planets* IV, edited by V. Mannings, A. P. Boss, S. S. Russell (University of Arizona Press, Arizona 2000), p. 1159.
[4] J. M. Sunshine *et al.*, Science **311**, 1453 (2006).
[5] L. Biermann, Z. Astrophys. **29**, 274B (1951).
[6] H. Alfven, Tellus **9**, 92 (1957).
[7] L. Biermann, B. Brosowski, and H. U. Schmidt, Sol. Phys. **1**, 254 (1967).
[8] D. A. Mendis, H. L. F. Houpis, and M. L. Marconi, Fundam. Cosm. Phys. **10**, 2 (1985).
[9] K. Szegő *et al.*, Space Sci. Rev. **94**, 429 (2000).
[10] T. I. Gombosi, in *Magnetotails in the Solar System*, American Geophysical Union Geophysical Monograph Series Vol. 207, edited by A. Keiling, C. M. Jackman, and P. A. Delamere (John Wiley & Sons, Inc., Hoboken, 2015), pp. 169–188.
[11] G. Haerendel, G. Paschmann, W. Baumjohann, and C. W. Carlson, Nature (London) **320**, 720 (1986).
[12] M. G. G. T. Taylor, C. Alexander, N. Altobelli, M. Fulle, M. Fulchignoni, E. Grün, and P. Weissman, Science **347**, 387 (2015).
[13] H. Nilsson *et al.*, Science **347**, 0571 (2015).
[14] Y. D. Jia, M. R. Combi, K. C. Hansen, T. I. Gombosi, F. J. Crary, and D. T. Young, Icarus **196**, 249 (2008).
[15] M. Rubin, C. Koenders, K. Altwegg, M. R. Combi, K.-H. Glassmeier, T. I. Gombosi, K. C. Hansen, U. Motschmann, I. Richter, V. M. Tenishev, and G. Tóth, Icarus **242**, 38 (2014).
[16] M. Rubin, M. R. Combi, L. K. S. Daldorff, T. I. Gombosi, K. C. Hansen, Y. Shou, V. M. Tenishev, G. Tóth, B. van der Holst, and K. Altwegg, Astrophys. J. **781**, 86 (2014).
[17] M. Rubin, T. I. Gombosi, K. C. Hansen, W.-H. Ip, M. D. Kartalev, C. Koenders, and G. Tóth, Earth Moon Planets **116**, 141 (2015).
[18] Z. Huang, G. Tóth, T. I. Gombosi, X. Jia, M. Rubin, N. Fougere, V. Tenishev, M. R. Combi, A. Bieler, K. C. Hansen, Y. Shou, and K. Altwegg, J. Geophys. Res. **121**, 4247 (2016).
[19] Y. Shou, M. Combi, G. Toth, V. Tenishev, N. Fougere, X. Jia, M. Rubin, Z. Huang, K. Hansen, T. Gombosi, and A. Bieler, Astrophys. J. **833**, 160 (2016).
[20] N. Gortsas, U. Motschmann, E. Kührt, J. Knollenberg, S. Simon, and A. Boesswetter, Ann. Geophys. **27**, 1555 (2009).
[21] S. Wiehle, U. Motschmann, N. Gortsas, K.-H. Glassmeier, J. Müller, and C. Koenders, Adv. Space Res. **48**, 1108 (2011).
[22] C. Koenders, K.-H. Glassmeier, I. Richter, U. Motschmann, and M. Rubin, Planet. Space Sci. **87**, 85 (2013).
[23] C. Koenders, K.-H. Glassmeier, I. Richter, H. Ranocha, and U. Motschmann, Planet. Space Sci. **105**, 101 (2015).
[24] E. Behar, J. Lindkvist, H. Nilsson, M. Holmström, G. Stenberg-Wieser, R. Ramstad, and C. Götz, Astron. Astrophys. **596**, A42 (2016).
[25] C. Koenders, C. Goetz, I. Richter, U. Motschmann, and K.-H. Glassmeier, Mon. Not. R. Astron. Soc. **462**, S235 (2016).
[26] C. Koenders, C. Perschke, C. Goetz, I. Richter, U. Motschmann, and K. H. Glassmeier, Astron. Astrophys. **594**, A66 (2016).
[27] G. Clark, T. W. Broiles, J. L. Burch, G. A. Collinson, T. Cravens, R. A. Frahm, J. Goldstein, R. Goldstein, K. Mandt, P. Mokashi, M. Samara, and C. J. Pollock, Astron. Astrophys. **583**, A24 (2015).

[28] T. W. Broiles *et al.*, J. Geophys. Res. **121**, 7407 (2016).
[29] H. Madanian, T. E. Cravens, A. Rahmati, R. Goldstein, J. Burch, A. I. Eriksson, N. J. T. Edberg, P. Henri, K. Mandt, G. Clark, M. Rubin, T. Broiles, and N. L. Reedy, J. Geophys. Res. **121**, 5815 (2016).
[30] S. Markidis, G. Lapenta, and Rizwan-uddin, Math. Comput. Simul. **80**, 1509 (2010).
[31] R. J. Mason, J. Comput. Phys. **41**, 233 (1981).
[32] J. U. Brackbill and D. W. Forslund, J. Comput. Phys. **46**, 271 (1982).
[33] G. Lapenta, J. U. Brackbill, and P. Ricci, Phys. Plasmas **13**, 055904 (2006).
[34] T. E. Cravens, Am. Geophys. Union Geophys. Monograph Ser. **61**, 27C (1991).
[35] K. E. Mandt *et al.* Mon. Not. R. Astron. Soc. **462**, S9 (2016).
[36] J. Deca, A. Divin, B. Lembège, M. Horányi, S. Markidis, and G. Lapenta, J. Geophys. Res. **120**, 6443 (2015).
[37] K. C. Hansen, T. Bagdonat, U. Motschmann, C. Alexander, M. R. Combi, T. E. Cravens, T. I. Gombosi, Y.-D. Jia, and I. P. Robertson, Space Sci. Rev. **128**, 133 (2007).
[38] A. Bret and M. E. Dieckmann, Phys. Plasmas **17**, 032109 (2010).
[39] T. I. Gombosi, M. Horanyi, K. Kecskemety, T. E. Cravens, and A. F. Nagy, Astrophys. J. **268**, 889 (1983).
[40] A. Bieler *et al.*, Astron. Astrophys. **583**, A7 (2015).
[41] N. J. T. Edberg *et al.*, Geophys. Res. Lett. **42**, 4263 (2015).
[42] M. Volwerk *et al.*, Ann. Geophys. **34**, 1 (2016).
[43] I. Richter *et al.*, Ann. Geophys. **33**, 1031 (2015).
[44] B. U. Ö. Sonnerup, in *Solar System Plasma Physics*, edited by L. J. Lanzerotti, C. F. Kennel, and E. N. Parker (North-Holland Publishing Co., Amsterdam, 1979), pp. 45–108.
[45] T. W. Broiles, J. Burch, K. Chae, G. Clark, T. Cravens, A. Eriksson, S. Fuselier, R. Frahm, S. Gasc, R. Goldstein, P. Henri, C. Koenders, G. Livadiotis, K. Mandt, P. Mokashi, Z. Nemeth, E. Odelstad, M. Rubin, and M. Samara, Mon. Not. R. Astron. Soc. **462**, S311 (2016).
[46] H. Nilsson *et al.*, Astron. Astrophys. **583**, A20 (2015).
[47] A. Divin, J. Deca, P. Henri, A. Eriksson, S. Markidis, and M. Horányi, in *Proceedings of the American Geophysical Society (AGU) Fall Meeting* (2016).
[48] T. W. Broiles, J. L. Burch, G. Clark, C. Koenders, E. Behar, R. Goldstein, S. A. Fuselier, K. E. Mandt, P. Mokashi, and M. Samara, Astron. Astrophys. **583**, A21 (2015).
[49] E. Behar, H. Nilsson, G. S. Wieser, Z. Nemeth, T. W. Broiles, and I. Richter, Geophys. Res. Lett. **43**, 1411 (2016).
[50] A. Divin, J. Deca, P. Henri, A. Eriksson, S. Markidis, and M. Horányi, Mon. Not. R. Astron. Soc. (to be published)
[51] A. I. Eriksson *et al.*, Astron. Astrophys. (to be published).
[52] P. Meier, K.-H. Glassmeier, and U. Motschmann, Ann. Geophys. **34**, 691 (2016).
[53] E. Vigren, M. Galand, A. I. Eriksson, N. J. T. Edberg, E. Odelstad, and S. J. Schwartz, Astrophys. J. **812**, 54 (2015).
[54] T. E. Cravens, T. I. Gombosi, B. E. Gribov, M. Horanyi, K. Kecskemety, A. Korosmezey, M. L. Marconi, D. A. Mendis, A. F. Nagy, R. Z. Sagdeev, V. I. Shevchenko, V. D. Shapiro, and K. Szego, *Role of Electric Fields in the Cometary Environment* (Hungarian Academy of Science, Budapest 1984).
[55] E. Vigren and A. I. Eriksson, Astron. J. **153**, 150 (2017).
[56] C. Goetz, C. Koenders, I. Richter, K. Altwegg, J. Burch, C. Carr, E. Cupido, A. Eriksson, C. Güttler, P. Henri, P. Mokashi, Z. Nemeth, H. Nilsson, M. Rubin, H. Sierks, B. Tsurutani, C. Vallat, M. Volwerk, and K.-H. Glassmeier, Astron. Astrophys. **588**, A24 (2016).
[57] P. Henri, X. Vallières, C. Goetz, I. Richter, K.-H. Glassmeier, M. Galand, M. Rubin, A. Eriksson, Z. Nemeth, E. Vigren, A. Beth, J. Burch, C. Carr, H. Nilsson, B. Tsurutani, and G. Wattieaux (to be published).